Flight Testing and Preliminary Analysis for Global System Identification of Ornithopter Dynamics Using On-board and Off-board Data

Armanini, Sophie; Karasek, Matej; de Visser, Coen; de Croon, Guido; Mulder, Max

DOI
10.2514/6.2017-1634

Publication date
2017

Document Version
Accepted author manuscript

Published in
AIAA Atmospheric Flight Mechanics Conference, 2017

Citation (APA)
Armanini, S., Karasek, M., de Visser, C., de Croon, G., & Mulder, M. (2017). Flight Testing and Preliminary Analysis for Global System Identification of Ornithopter Dynamics Using On-board and Off-board Data. In *AIAA Atmospheric Flight Mechanics Conference, 2017: 5-9 June 2017, Denver, Colorado* Article AIAA 2017-1634 American Institute of Aeronautics and Astronautics Inc. (AIAA). https://doi.org/10.2514/6.2017-1634

This is an Accepted Manuscript of an article published in: 23rd AIAA/CEAS Aeroacoustics Conference 5-9 June 2017, Denver, Colorado. ISBN: 978-1-62410-448-0
Available online: https://arc.aiaa.org/doi/10.2514/6.2017-1634

Flight testing and preliminary analysis for global system identification of ornithopter dynamics using on-board and off-board data

S.F. Armanini*, M. Karásek †, C.C. de Visser‡, G.C.H.E. de Croon*, M. Mulder§
Delft University of Technology, 2629HS Delft, The Netherlands.

Bioinspired flapping-wing robots allow for unprecedented manoeuvrability and versatility, and increasingly small and light designs, with significant potential for flight in tight or cluttered spaces. For efficient design, operation and control of such vehicles, fully exploiting their potential and allowing for flight in a wide range of conditions, it is paramount to explore and model their dynamics across their intended flight envelope. However, due the complex flapping-flight mechanisms and limited availability of free-flight data, global models are not yet available, particularly models based on real flight data and simple enough to be applicable in practice. This paper discusses a set of free-flight tests conducted with an ornithopter to, firstly, investigate its dynamics in a range of different flight conditions, and, secondly, provide a basis for global model identification, important for advanced controller development, simulation and performance evaluations. The obtained results are presented and system identification is used to provide insight into the dynamics of the ornithopter in different flight conditions. Additionally, the flight testing process is discussed, focusing on acquiring data suitable for identification and analysis of flapping-wing vehicles, specifically. This includes fusing on-board IMU and off-board optical tracking data, to obtain not only a higher quality and reliability, but also accurate high-frequency measurements that can be used to analyse time-resolved flapping effects in free flight and during manoeuvres.

Nomenclature

a_x, a_y, a_z	=	accelerations measured by IMU
b_{ax}, b_{ay}, b_{az}	=	accelerometer biases
b_p, b_q, b_r	=	gyroscope biases
f	=	flapping frequency
g	=	acceleration due to gravity
H	=	Jacobian of the measurement equation
$I_{xx}, I_{zz}, I_{yy}, I_{xy}, I_{yz}, I_{zx}$	=	body moments of inertia
K	=	Kalman gain
m	=	mass
P	=	estimated measurement error covariance matrix
p, q, r	=	angular rates in body-fixed coordinates
Q	=	process noise covariance matrix

*PhD Student, Control & Simulation Division, Faculty of Aerospace Engineering, Kluyverweg 1, 2629HS Delft, The Netherlands. s.f.armanini@tudelft.nl. AIAA Student Member.
†Postdoctoral Researcher, Control & Simulation Division, Faculty of Aerospace Engineering, Kluyverweg 1, 2629HS Delft, The Netherlands.
‡Assistant Professor, Control & Simulation Division, Faculty of Aerospace Engineering, Kluyverweg 1, 2629HS Delft, The Netherlands. AIAA Member.
§Professor, Control & Simulation Division, Faculty of Aerospace Engineering, Kluyverweg 1, 2629HS Delft, The Netherlands. AIAA Associate Fellow.

R	=	measurement noise covariance matrix
u_b, v_b, w_b	=	velocities in body-fixed coordinates
v_{ub}, v_{vb}, v_{wb}	=	measurement noise in velocity measurements
v_Φ, v_Θ, v_Ψ	=	measurement noise in attitude measurements
w_{ax}, w_{ay}, w_{az}	=	process noise in accelerations
w_p, w_q, w_r	=	process noise in rates
X_i, Z_i, M_i	=	stability and control derivatives in standard notation
x_b, y_b, z_b	=	(positions in) body-fixed coordinate system
x_i, y_i, z_i	=	(positions in) inertial coordinate system
α	=	angle of attack
Γ	=	discrete input matrix
δ_e	=	elevator deflection
$\delta_{e,CMD}$	=	commanded elevator deflection
$\delta_{f,CMD}$	=	commanded flapping frequency
Φ, Θ, Ψ	=	Euler angles
$\mathbf{\Psi}$	=	discrete state transition matrix

I. Introduction

Flapping-wing flyers have a remarkable performance at very low Reynolds numbers: they are highly manoeuvrable, power efficient and versatile, typically being able to fly in a wide range of different conditions, extending from hover to fast forward flight. Hence bio-inspired flapping-wing micro aerial vehicles (FWMAVs) are being researched extensively, and are expected to allow for novel applications that are not achievable with conventional fixed-wing or rotary-wing aircraft. However, flapping-wing mechanisms are highly complex, due to the unsteady aerodynamics, involving phenomena such as wake-capture and leading edge vortices, and time-varying dynamics. While significant insight is now available on both fronts, thanks to studies on insects and birds[1,2,3,4,5] , and, more recently, increasingly on robotic test platforms,[6,7,8,9,10,11,12,13,14] the high complexity of flapping flight still poses a considerable challenge to FWMAV development. Additionally, a considerable difficulty is still obtaining realistic experimental data, particularly in free flight and in different flight regimes. Studies have found discrepancies between free-flight and wind tunnel data,[15,16,17] so that realistic insight for free flight ideally should be obtained in free-flight conditions.

For the reasons mentioned, analysis and modelling of flapping flight remains challenging, especially obtaining simple, computationally efficient models that can yield basic insight and be used for design and control in real-life applications. Hence, when flight data is obtainable, an attractive alternative to often complex and computationally expensive theoretical or numerical models is system identification. Previous system identification efforts[18,19,20,21,22,23,24] showed that a data-driven approach can yield realistic but simple models, as well as new insight, for a novel and complex type of vehicle, not known in great depth. However relatively limited work has been done in this field so far, partly due to the difficulty of obtaining suitable data. Additionally, existing identification work on flapping-wing flyers is limited to specific flight conditions. This limitation is shared by most low-order dynamic and aerodynamic models currently available, which typically have a limited applicability range, e.g. hover,[25,26] and/or have not been validated in different conditions with free-flight data.[27,28]

This is a limitation because one of the attractive features of ornithopters is in fact their ability to operate in different regimes, which can lead to very different flight properties. This could be exploited to allow the same vehicle to be used for different purposes, e.g. transitioning easily from rapid flight in an open area, to agile manoeuvring in a tight space, to hover. Knowing how a vehicle behaves in the different conditions it is intended to fly in is necessary for safe and efficient operation and to maximally exploit its potential, and is also useful *per se* as new insight into an unconventional type of flight mechanism is obtained. Furthermore, accurate, full flight-envelope models are highly valuable for design and advanced control.

Thus, there is currently a lack of insight into the changing dynamics of flapping-wing flyers in different conditions, and a lack of simple global models to represent these changes. Additionally, there is limited free-flight data available that might assist in addressing these gaps, and generally support improved understanding and further development of flapping-wing vehicles.

This paper discusses flight tests conducted, firstly, to investigate the flight dynamics of a flapping-wing vehicle in different conditions, secondly, to support full flight envelope model identification of the FWMAV, and, thirdly, to provide a comprehensive dataset for system identification and for in-depth analysis of time-resolved flapping-flight behaviour, thanks to the fusion of on-board IMU data and off-board optical tracking measurements. The flight testing process is discussed, focusing on relevant points for FWMAVs specifically, and a data fusion approach is used to improve the accuracy and resolution in the reconstructed states, and to allow also for the sub-flap cycle dynamics to be analysed in depth in free flight and during manoeuvres. System identification is then used to compute low-order, linear dynamic models in each of the flight regimes covered in the flight tests, and these models are applied to gain initial insight into the dynamics of the studied platform in different flight conditions.

This paper is organised as follows. Sec. II introduces the test vehicle used in this study, the flight testing setup and data acquisition hardware. Sec. III discusses the experiment design and flight test process, focusing on issues specific to FWMAVs and system identification, as well as on data fusion. Sec. IV discusses the main results obtained. The dynamics of the vehicle in different flight regimes are discussed and initial trends pointed out. Potential uses of the collected data for time-resolved modelling are also briefly mentioned. Sec. V closes the paper with a summary of the main findings and conclusions.

II. Experimental setup

A. Test vehicle

The platform used in this study is a four-winged ornithopter (cf. Fig. 1) with a 280mm wingspan, typical flapping frequencies in the range of 10-15Hz and a flight envelope ranging from near hover to fast forward flight. The mylar foil wings have an 'X'-configuration, allowing for increased lift production thanks to the clap-and-peel effect, while the T-shaped styrofoam tail leads to static stability and separates the bulk of the manoeuvring from the wing flapping, operating according to the same principles as a standard aircraft tail, with movable rudder and elevator surfaces. The same type of vehicle has been the subject of extensive previous research and detailed geometric properties and descriptions of the design can be found, e.g., in Refs.[29,30,31] The mass and inertia properties of the specific FWMAV used in these flight tests are presented in Table 2. Fig. 1(b) shows the orientation of the body-fixed coordinate system used in this study, defined to be centred at the centre of gravity (CG) of the platform. In contrast to convention, the z-axis is aligned with the fuselage – this was done to avoid attitude singularities, given the typically large pitch angle assumed in flight by this FWMAV.

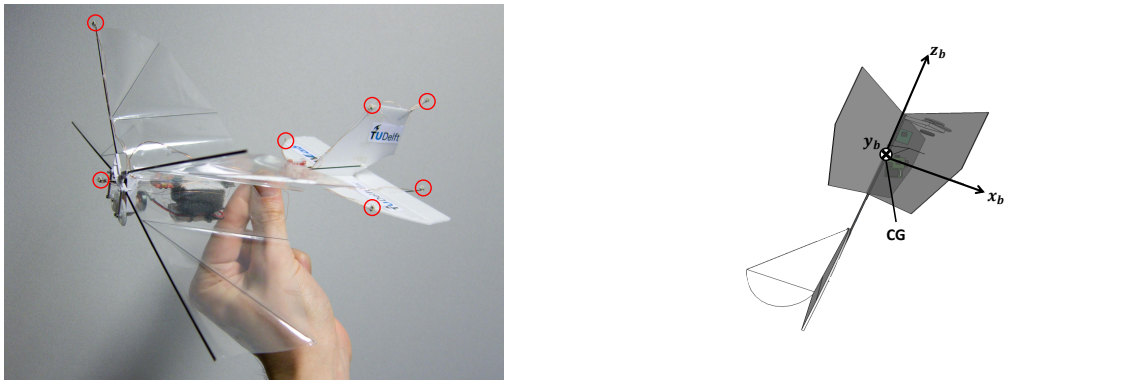

(a) Test platform (DelFly II[29])

(b) Body-fixed coordinate frame, centred at the CG

Figure 1: Test platform used in this study and body-fixed coordinate system x_b, y_b, z_b

B. Flight test setup and in-flight data acquisition

The test platform was flown in a 10m×10m×7m motion tracking facility (TU Delft *Cyberzoo*), equipped with 24 OptiTrack Flex13 cameras, and relevant measurements were acquired during flight using two different methods.

Table 2: Mass and inertia properties of the test platform

Property	Value
$m[g]$	23.5
$x_{CG}[mm]$ (below fuselage)	9.6
$y_{CG}[mm]$	0
$z_{CG}[mm]$ (from wing leading edge)	68.5
$I_{xx}, I_{yy}, I_{zz}[Nm^2]$	7.5E-05, 6.6E-05, 1.9E-05
$I_{xy}, I_{yz}, I_{xz}[Nm^2]$	0, 0, 8.5E-06

Firstly, the aforementioned optical tracking system (hereafter: "OptiTrack") was used to measure the positions of 7 active LED markers attached to the FWMAV at the locations illustrated in fig. 1(a). The four markers attached to the fuselage allowed for reconstruction of the position and orientation (quaternions) of the rigid body, while the remaining markers, on the wing leading edge, rudder and elevator allowed for reconstruction of the control surface deflections, and of the wing leading edge movement, hence the wing flap angle (ζ). The obtained measurements were transformed from the OptiTrack coordinate system to the body-fixed coordinate frame shown in fig. 1(b), and quaternions were transformed to Euler angles for easier interpretation. Note that the CG location does not coincide with the centre of the OptiTrack-defined body-coordinate system, which is based on geometry. This difference was considered when processing the data.

Secondly, on-board measurements were acquired by means of an inertial measurement unit (IMU). For the flight tests presented, the FWMAV was equipped with a 2.8g Lisa/S autopilot,[32] which includes a 6-axis MEMS IMU and a microcontroller unit (ARM Cortex-M3), allowing for open-source drone autopilot framework Paparazzi-UAV[33] to be run. The IMU was used to measure the linear accelerations and angular velocities of the vehicle, at a chosen sampling frequency of 512Hz. While sampling up to 1024Hz is possible, internal low-pass filtering at 256Hz implies that such sampling frequencies would not yield accurate additional information. Moreover, previous work with similar ornithopters showed that very high-frequency content becomes increasingly difficult to distinguish from noise.[34]

The IMU was attached to the body. Following the initial finding that the attachment mode influenced the measurements made, a block of foam was added between IMU and fuselage, to introduce damping and reduce unwanted vibrations. Small residual effects that remain despite the foam are being studied further, however these effects were found to be small after the aforementioned modification. The IMU measurements, as well as servo commands and motor speed, were logged using an SD card added to the autopilot. Further details on the hardware and flight test setup (e.g. calibration, synchronisation) can be found in.[35]

Table 3: Overview of relevant data obtained from each data acquisition system.

Data acquisition means	Measurements provided
OptiTrack	$x_i, y_i, z_i, \Phi, \Theta, \Psi, \delta_E, \zeta$
IMU	p, q, r, a_x, a_y, a_z
On-board additional	$\delta_{E,CMD}$, RPM

III. Experiment design and data processing

Based on the aims stated in sec. I, flight tests were devised to meet the following requirements: (i) cover a range of different flight conditions, (ii) provide data suitable for system identification and compatible with a local linear modelling approach, focused on a cycle-averaged level, and (iii) provide data potentially applicable also to study the time-resolved behaviour within each flap cycle. This section elucidates the process of obtaining useful data meeting these requirements. An overview is given of both the flight testing and the subsequent data processing, covering the following points: selection of test conditions and definition of flight procedures (sec. IIIA, III. B), experiment design (sec. III.C), and data processing (sec. III.D).

A. Test conditions and flight test overview

Preliminary tests on the same platform,[35] and previous research on similar vehicles,[31,36] were used to obtain an idea of the ornithopter's flight envelope and to establish a matrix of test conditions to fly in. Subsequently, this initial framework was adjusted based on observations made while flying. Initial tests suggested that typical flight conditions range from approximately 0.3m/s to 1.5m/s. In fact earlier tests[31] showed that the ornithopter can fly at much higher speeds of over 7m/s, however this requires shifting the CG (e.g. by physically moving parts of the platform such as the battery, or the wings and flapping mechanism). Future work will thus encompass including the CG as a model parameter, to yield insight into the dynamics with different CG locations and help establish advantageous CG locations for design. At this stage only one CG location was considered. An additional limitation regarding flight envelope coverage is constituted by the experimental setup. The limited size of the motion tracking arena where flights were conducted (cf. sec. II.B), implies that very high speeds entail both high risk of crashing and insufficient time for effective manoeuvring. Nonetheless, the available space allowed for a wide range of conditions to be covered, including the most commonly flown regimes. Finally, the current flight testing focused only on the longitudinal dynamics, hence trim conditions were defined in terms of angle of attack and velocity norm, and manoeuvres were designed only to influence the relevant states, i.e. velocities, pitch rate and pitch attitude (cf. sec.III. C).

Based on previous results and flight experience, 5 different steady flight conditions were chosen to conduct identification manoeuvres in. The trim settings and corresponding steady-state velocity, angle of attack and flapping frequency are given in table 4. Given that flights were conducted manually, with only the input signals for identification being executed by the autopilot, effectively a small range around each condition listed in the table was covered. An overview of the actual conditions explored can be found in sec. IV, fig. 8.

Table 4: Flight conditions where system identification manoeuvres were conducted

Condition #	Elevator trim [%]	Flap frequency [Hz]	Angle of attack [deg]	Velocity [m/s]
1	-40	13.8	75	0.4
2	-30	13.8	65	0.5
3	0	13.3	50	0.75
4	20	12.6	45	0.9
5	30	12.3	40	1.1

B. Flight test execution

To conduct manoeuvres suitable for system identification, the Lisa/S autopilot board and Paparazzi autopilot were used to pre-programme the input signals according to the desired specifications, and to execute these automatically during flight, when triggered by the pilot. Flights were conducted according to the following procedure. The elevator was fixed at a specific position, giving the trim setting, and small adjustments to the throttle were then made by the pilot to establish a steady condition. Once a stationary condition was attained, the pilot could trigger the pre-programmed input signals by means of a switch. No other inputs were made during the identification manoeuvre and while the effects of the input were acting on the platform, until the aircraft reached the edge of the flight arena, at which point the pilot intervened and the procedure was repeated. Each flight lasted approximately three to four minutes and included several separate manoeuvres. Prior to each flight, a series of static measurements were executed for calibration purposes, particularly for alignment between IMU and optical tracking system, and to enable accurate measurement of the control surface deflections.[35]

C. Input design remarks

Having selected the test conditions and established the basic procedure and setup for executing the flights, suitable test manoeuvres for identification were designed. While input design is a well-established field and many guidelines exist for aircraft system identification experiments, novel systems can present a challenge, due to the more limited *a priori* knowledge and experience available. This is the case for flapping-wing robots,

where (i) the dynamics are not known in great detail, (ii) free-flight data are not easily obtainable and thus there is still little experience with and data from flight testing, and (iii) the flapping motion introduces an additional complication.

Different approaches for input design include: computing in some way optimal inputs based on a priori knowledge of the system,[37,38] choosing input signals based on approximate or qualitative prior knowledge and trial and error testing, or simply exciting as many frequencies as possible using heuristic signals such as frequency sweeps. In the interest of simplicity, and given that some, but not comprehensive, prior knowledge was available on the studied ornithopter, an engineering approach was chosen to design simple multistep inputs. We started from standard aircraft guidelines,[39,40] and adjusted these with the help of insight from previous work and preliminary flight tests to obtain more effective results.

A preliminary decision was to use elevator deflections as sole input in the current tests. This is because they represent the most effective and straightforward way of exciting most of the ornithopter dynamics, and hence a useful starting point, however future work will also encompass throttle manoeuvres that vary the flapping frequency. As signal type, doublets were selected, due to their simple execution and symmetry, which makes the ornithopter more likely to remain close to its initial stationary condition following the manoeuvre. Compared to 211 or 3211 signals with equally long pulses, doublets are also shorter in duration, and given the limited size of the flight arena, this is advantageous as it allows for longer response times. Previous tests with a similar ornithopter also showed that doublets provided sufficient excitation.[31]

The duration and amplitude of the inputs were tuned based on a number of interrelated considerations. Firstly, the input signal must provide adequate excitation of the frequency range of interest. Evidently, a larger, longer input provides more information, as long as it continues to excite the aircraft, but it also requires longer tests and takes the vehicle further away from its steady condition, possibly violating linearity assumptions. On the other hand, small, very rapid signals can lead to an unclear response and significant noise influence.

Secondly, to allow the cycle-averaged dynamics to be identified effectively on their own, the input must be such that the body dynamics are distinct from the flapping-related oscillations. The flapping motion induces oscillations of the body, that, depending on the amount of filtering and the particular state, can have significant amplitudes (cf. fig. 2). If only the cycle-averaged dynamics are considered, then the flapping-related dynamics effectively represent a disturbance - and can imply a large signal-to-noise ratio, which negatively impacts the results. This for instance can require large input signals. Indeed it was found that, because of this and the particular dynamics of the system (discussed subsequently), relatively large inputs are required compared to typical inputs used for linear model identification with fixed-wing aircraft.[41,42,43] This, however, may conflict with the linearity requirement. Alternatively, a solution may be to minimise this problem by completely filtering out the flapping content prior to identification.[24]

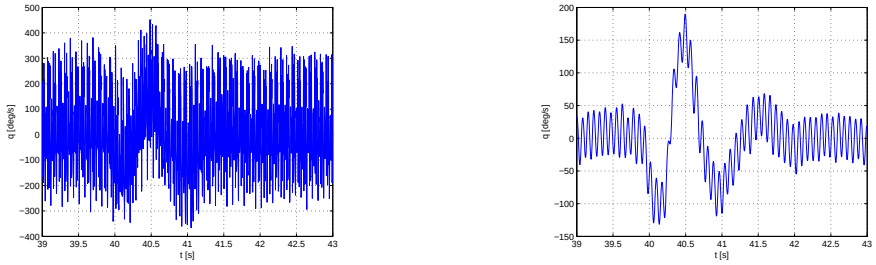

(a) Filtered at 50Hz

(b) Filtered at 15Hz, just above the flapping frequency

Figure 2: Sample of IMU-measured pitch rate q, low-pass filtered at different frequencies, highlighting the sometimes very large flapping-induced oscillations, as compared to the body oscillations.

Thirdly, if a linear modelling approach is considered, the aircraft must remain close to its initial, steady condition. This implies that the chosen manoeuvre must be somewhat symmetrical and not excessively long or large. Additionally, and lastly, to allow for linear modelling, it is important to fly in a steady condition in the first place, i.e. to achieve and maintain a sufficiently steady initial condition prior to execution of the manoeuvres. In practice this can be challenging to do manually, particularly for a vehicle that is continually

oscillating and flying in a limited space, particularly considering the effect of air draughts and the need to re-stabilise after every turn. Trimming manually means that the initial condition is not always completely steady, and that it is difficult to re-create the exact same conditions repeatedly. This is enhanced by the fact that slightly different velocity/flapping-frequency/attitude combinations are possible with the same elevator trim.

The space restrictions mean that the time available for each manoeuvre is limited, and this time must include both a sufficient steady-state *run-in*, and sufficient time for the input to be executed and its effects observed. Insufficient measurement time leads to more variation in the identified dynamics, as some components may not be observed effectively. At the same time, the edge of the flight space is reached rapidly, which implies frequent sharp turns that take the vehicle away from its steady condition, requiring time for a steady state to be reached again. Large rudder inputs for instance led to considerable disturbance, often making the successive manoeuvre unusable for identification. These requirements are in conflict – more time to stabilise leaves less time for the response, and the problem becomes increasingly significant in faster flight. A possible solution may be to fly in non-restricted space, using IMU measurements only. However, this necessitates sensor fusion algorithms that are based on on-board measurements alone,[?] possibly at the cost of lower quality, and would also require an approach for velocity estimation, as integrated accelerometer measurements alone are not suitable for this. A further alternative may be to still only track in the limited tracking area, but use additional, untracked space to *reach* steady conditions, thus using the tracking space exclusively for the useful manoeuvre.

The amplitude and duration of the input signals were selected on the basis of all the above considerations, finally leading to signals like that shown in fig. 4.

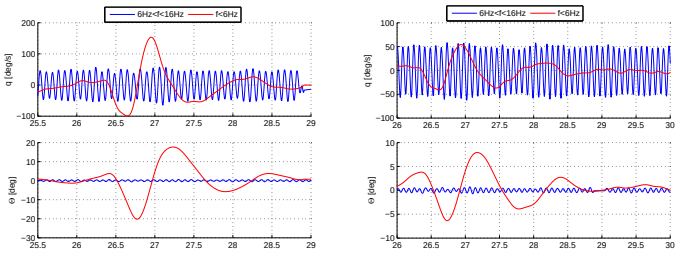

(a) 35° elevator deflection (b) 10° elevator deflection

Figure 3: Effect of different input amplitudes on the pitch attitude and rate: comparison of flapping-related (blue) and cycle-averaged (red) components

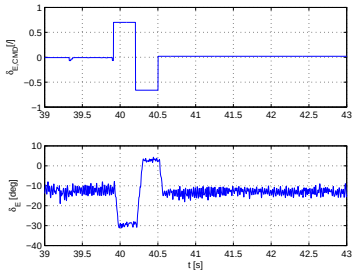

Figure 4: Example of elevator signal used for identification, in terms of command and resulting deflection.

Previous work on the same ornithopter design suggested natural frequencies of approximately 1Hz[44,23] in typical flight conditions - while this is only an indicative value and will change in different flight regimes, it gives an initial reference for input design. Based on frequency-domain analysis, approximate suitable durations for a signal[45] can be derived, such that the power content peaks around the expected natural frequency. From this type of analysis combined with initial tests, a duration of 0.35s per pulse in the doublet was selected. This was also found to be suitably short for the time and space constraints discussed, and generally allowed for the vehicle not to move away from its stationary condition. While different values will be more effective in different flight conditions, to minimise the test times and since no quantitative information was available on this, the same duration was used in all tests.

The amplitude was then chosen to provide sufficient excitation, while considering the restrictions discussed. $30 - 40$deg elevator deflections were used in the final tests, with smaller amplitudes becoming necessary where more of the elevator deflection range was needed to maintain the trimmed condition. As mentioned, both deflections and responses are considerably larger than is typical for standard aircraft in a linear modelling context. Inputs of a few degrees lead to responses in the same order of magnitude as the flapping-related oscillations, particularly in the linear and angular velocities. Moreover, the different dynamics play a role - FWMAVs easily reach extremely large angular velocities, i.e. even a small input will lead to small but extremely rapid changes in attitude. Compared to a standard aircraft, the same change in attitude may be achieved an order of magnitude more rapidly. Nonetheless, while the current, fairly large inputs were found to yield accurate results, future work should investigate how this dynamic behaviour affects

linearity assumptions. To improve the signal-to-noise ratio, when analysing the cycle-averaged dynamics, the flapping-related content was wholly filtered out. This was found to improve the results, and was significantly less likely to lead to convergence problems in the estimation algorithm.

To maximise the available time for each manoeuvre, diagonal trajectories were flown across the tracking space. Manoeuvres were conducted in the central part of the flight arena, allowing enough time for the vehicle to stabilise after precedent turns, but still providing enough time for the effects to be observed.

D. Data processing and fusion

The flight test setup described allowed us to combine on-board IMU measurements and external optical tracking measurements, to obtain a highly accurate and informative dataset, suitable specifically for analysing and modelling flapping-wing vehicles. In particular, this not only leads to the usual favourable results of sensor fusion, e.g. higher accuracy and reliability, but also allows for accurate high-frequency measurements, indispensable for in-depth analysis of flapping-wing flight and the short time-scale mechanisms involved.

Optical tracking yields sub-millimetre precision and reliable measurements, whose accuracy does not deteriorate over time. The main drawbacks include: (i) generally relatively low sampling frequencies for the considered purpose, e.g. here 120Hz; (ii) presence of glitches and occasionally untracked or misattributed markers, e.g. due to light disturbance; and (iii) exclusive measurement of position and attitude, meaning rates must be computed via numerical differentiation, which introduces considerable noise.[15] The low acquisition frequency, in particular, means that even for the relatively low flapping frequency of the studied ornithopter (10-15Hz), only approximately 8-12 measurements are made during each flap cycle. As can be seen in fig. 6(a), this leads to a relatively low resolution, hence accurate analysis at a sub flap-cycle time scale is possible only with great limitations.

By contrast, IMU measurements are typically gathered at very high sampling frequencies, here up to 1024Hz. This represents a significant advantage for looking at the sub flap-cycle level. Additionally, IMU devices provide relatively accurate measurements over short time scales and are not prone to glitches – all of which can be exploited to generally enhance the reliability of the resulting dataset. The major drawback is integration drift, as well as increased noise and the possibility of biases, which must be computed during calibration procedures and/or estimated in flight. Additionally, in the current experimental setup the way the IMU is attached to the body also represents a potential source of error.

While each of the used measurement devices has limitations, combining their output allows for improved reliability, thanks to redundant information, the availability of more direct measurements, fewer issues with noise propagation, glitches and missing data, and more accurate and informative high-frequency data. In the rest of this section the data fusion approach is outlined and the resulting data are briefly discussed.

1. *Filter design for data fusion*

An extended Kalman filter (EKF) was designed to fuse the IMU and optical tracking-provided data. The EKF is an extension of the linear Kalman filter that is applicable to nonlinear systems, with the drawback that a global optimal solution cannot be guaranteed, and divergence may occur, e.g. due to inadequate initialisation. Improvements can be attained e.g. using iterated Kalman filters, however, for the present application, an EKF was found to provide accurate results. The EKF is documented comprehensively in the literature, thus only the main equations are given here, for a nonlinear state-space system of the form:

$$x(t_{k+1}) = f(x_k, u_k, t_k) + g(u_k, t_k) + w(t_k) \tag{1}$$

$$z(t_k) = h(x, u, t_k) + v(t_k) \tag{2}$$

where x denotes the states, u the input, z the output, z the measured output, w the process noise and v the measurement noise. The process and measurement noise are assumed to be white and Gaussian, and are characterised by covariance matrices Q and R, respectively. The filter is then given by the following equations.

Prediction:

$$\hat{x}_{k+1,k} = f(\hat{x}_{k,k}, u_k, t) \tag{3}$$

$$P_{k+1,k} = \Phi_{k+1,k} P_{k,k} \Phi_{k+1,k}^T + \Gamma_{k+1,k} Q_{k+1} \Gamma_{k+1,k}^T \tag{4}$$

Innovation:

$$K_{k+1} = P_{k+1,k} H_k^T [H_k P_{k+1,k} H_k^T + R_{k+1}]^{-1} \tag{5}$$

$$\hat{x}_{k+1,k+1} = \hat{x}_{k+1,k} + K_{k+1}[z_{k+1} - h(\hat{x}_{k+1,k}, u_{k+1})] \tag{6}$$

$$P_{k+1,k+1} = P_{k+1,k} - K_{k+1} H_k P_{k+1,k}^T \tag{7}$$

where Φ and Γ are the discretised state transition and input matrices for the linearised system at step k, P is the estimated measurement error covariance matrix, K is the Kalman gain, and H is the Jacobian of the measurement equation.

The filter designed in this study estimates the body attitude and velocities, as well as accelerometer and gyro biases, using IMU data as input variables and optitrack data as output measurements. Given that on the test platform, as on most current FWMAVs, no on-board velocity measurement was available, the velocities fed to the EKF as measurements (u_b^*, v_b^*, w_b^*) were in fact calculated from the OptiTrack-measured positions, via numerical differentiation and necessary coordinate transforms, using the attitude computed from the OptiTrack-measured quaternions.

$$\begin{bmatrix} u_b^* \\ v_b^* \\ w_b^* \end{bmatrix} = \begin{bmatrix} \cos\Psi\cos\Theta & \cos\Phi\sin\Psi + \cos\Psi\sin\Phi\sin\Theta & \sin\Phi\sin\Psi - \cos\Phi\cos\Psi\sin\Theta \\ -\cos\Theta\sin\Psi & \cos\Phi\cos\Psi - \sin\Phi\sin\Psi\sin\Theta & \cos\Psi\sin\Phi + \cos\Phi\sin\Psi\sin\Theta \\ \sin\Theta & -\cos\Theta\sin\Phi & \cos\Phi\cos\Theta \end{bmatrix} \times \begin{bmatrix} \dot{x} \\ \dot{y} \\ \dot{z} \end{bmatrix}_{OT}$$

The states, inputs, outputs and noise terms of the filter, according to eq. 8, are thus,

$$\begin{aligned} x &= [\Phi \;\; \Theta \;\; \Psi \;\; u_b \;\; v_b \;\; w_b \;\; b_p \;\; b_q \;\; b_r \;\; b_{ax} \;\; b_{ay} \;\; b_{az}]^T \\ u &= [p \;\; q \;\; r \;\; a_x \;\; a_y \;\; a_z]^T \\ z &= [\Phi \;\; \Theta \;\; \Psi \;\; u_b^* \;\; v_b^* \;\; w_b^*]^T \\ v &= [v_\Phi \;\; v_\Theta \;\; v_\Psi \;\; v_{ub} \;\; v_{vb} \;\; v_{wb}]^T \\ w &= [w_p \;\; w_q \;\; w_r \;\; w_{ax} \;\; w_{ay} \;\; w_{az}]^T \end{aligned}$$

and the process and measurement equations are:
Process equations:

$$\dot{\Phi} = (p - b_p) + (q - b_q)\sin\Phi\tan\Theta + (r - b_r)\cos\Phi\tan\Theta \tag{8}$$

$$\dot{\Theta} = (q - b_q)\cos\Theta - (r - b_r)\sin\Phi \tag{9}$$

$$\dot{\Psi} = (q - b_q)\sin\Phi\sec\Theta + (r - b_r)\cos\Phi\sec\Theta \tag{10}$$

$$\dot{u}_B = (r - b_r)v_b - (q - b_q)w_b - g\sin\Theta + a_x - b_{ax} \tag{11}$$

$$\dot{v}_B = -(r - b_r)u_b + (p - b_p)w_b + g\sin\Phi\cos\Theta + a_y - b_{ay} \tag{12}$$

$$\dot{w}_B = (q - b_q)u_b - (p - b_p)v_b + g\cos\Phi\cos\Theta + a_z - b_{az} \tag{13}$$

$$\dot{b}_p = 0 \tag{14}$$

$$\dot{b}_q = 0 \tag{15}$$

$$\dot{b}_r = 0 \tag{16}$$

$$\dot{b}_{ax} = 0 \tag{17}$$

$$\dot{b}_{ay} = 0 \tag{18}$$

$$\dot{b}_{az} = 0 \tag{19}$$

Measurement equations

$$\Phi_m = \Phi + v_\Phi \tag{20}$$

$$\Theta_m = \Theta + v_\Theta \tag{21}$$

$$\Psi_m = \Psi + v_\Psi \tag{22}$$

$$u_b^* = u_b + v_x \tag{23}$$

$$v_b^* = v_b + v_y \tag{24}$$

$$w_b^* = w_b + v_z, \tag{25}$$

where $[\Phi, \Theta, \Psi]$ are the Euler angles, $[p, q, r]$ are the roll, pitch and yaw rates, $[u_b, v_b, w_b]$ are the body-frame velocities, $[a_x, a_y, a_z]$ are the accelerometer-measured accelerations, $[b_p, b_q, b_r, b_{ax}, b_{ay}, b_{az}]$ are the sensor biases of the gyroscope and accelerometer, $[v_{ub}, v_{vb}, v_{wb}, v_\Phi, v_\Theta, v_\Psi]$ are the measurement noise in the measured

velocities and attitudes, and $[w_p, w_q, w_r, w_{ax}, w_{ay}, w_{az}]$ are the process noise in the rates and accelerations. Asterisk superscripts indicate terms that are not directly measured but calculated from measurements, as discussed.

The process and measurement noise matrices, Q and R, were initially based on the actual noise characteristics of the measurements, and then adjusted based on the known or expected behaviour of OptiTrack and IMU, and on the resulting outcome. Considering the desired outcome and known behaviour of the sensors, results were found to be most effective when OptiTrack measurements were favoured. Based on the previous discussion, a desirable solution is one where sufficient high-frequency content is left in the fused data, thanks to the IMU contribution, while the slow time-scale evolution largely follows that of the OptiTrack. Thus the underlying idea is to use the optical tracking data as a basis, particularly on a cycle-averaged and long-term level, while using IMU data to (i) compensate for glitches in the tracking and (ii) provide accurate high-frequency content. Additionally, the IMU provides useful direct measurements of the rates and accelerations, unavailable from the tracking system.

Hence, the Q and R matrices were tuned to give more weight to the OptiTrack data. To select effective values, we considered, firstly, the amplitude of the flapping-related oscillations, and, secondly, the innovation errors and convergence behaviour. The flapping-related oscillations were in some cases observed to have larger amplitudes in IMU than in OptiTrack measurements. This may be due to the effect of the IMU mount, and for the velocities, different sensitivities of the accelerometer along different axes may also have an effect. Nonetheless, comparing forces estimated from the IMU alone to wind tunnel data[35] showed an overall adequate agreement, with minor discrepancies. Hence at sub-flap cycle level, the two measurements were given similar weighting.

Comparing the innovation errors to the uncertainty bounds predicted by the EKF, it was found that while reducing R and increasing Q leads to increasingly small innovation errors and faster filter convergence, eventually this leads to a significant discrepancy between innovation errors and error bounds predicted by the filter. Thus, a compromise was found, where the errors and estimated error bounds are small, but the former are still contained within the latter. Even a very significantly higher weighting of the OptiTrack measurements was found to allow for high-frequency content to be taken over from the IMU measurements, while also leading to small innovation errors and rapid convergence.

2. Data fusion results

Fig. 5 shows an example of fused data. It can be seen that an accurate result is achieved: in the long term there is significant agreement between the OptiTrack data and the EKF result, while at small time scales, the IMU sensor readings are used to obtain a high-resolution, accurate result, that improves significantly on what could be achieved with the the OptiTrack alone. The detailed views in fig. 6 highlight the increased information that can be obtained at high frequencies.

Fig. 7 shows that the innovation errors are mostly contained within the estimated error bounds, suggesting an effective filter implementation. Errors in the estimated attitude are typically approximately 1-2° during flight, and below 0.2° in the static case, however errors in the velocities are still relatively high during flight, reaching up to 0.1m/s, possibly due to the numerical derivatives used as measurements. More effective tuning will be explored to improve this result. Bias terms were found to approximately converge in the static case, and only vary slightly during flight. Values were found to be small, most likely thanks to the calibration procedures conducted prior to each flight, so that neglecting these terms may not have a significant impact. Nonetheless, the possibility of biases should be considered in a general setup.

Further testing and analysis of the sensors is required to draw conclusions on the remaining discrepancies between IMU and OptiTrack measurements mentioned above. Additionally, the velocity estimation can still be improved. The current setup should however be suitable for most modelling and identification work. The obtained data are accurate, contain detailed high-frequency information, and entail increased reliability due to the merging of separate data sources.

IV. Flight test results and dynamic analysis

Tests were conducted around the conditions defined in table 4. Due to the manual flying and the duration of the flights, there was some play around these nominal conditions. Fig. 8 gives a visual overview of the actual coverage attained in the tests, mapping the states and inputs of all the flown manoeuvres against

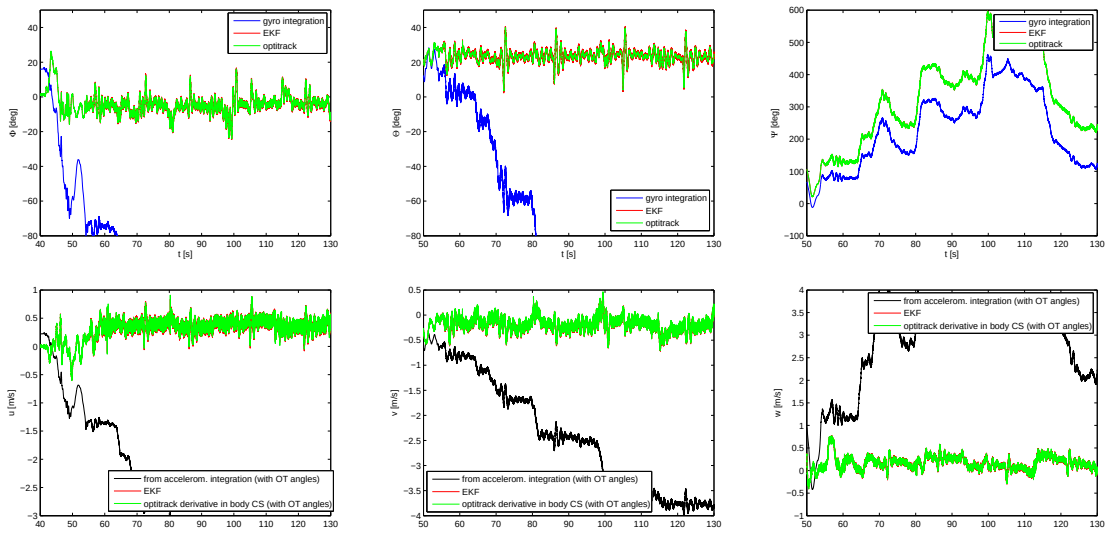

Figure 5: EKF results. Comparison of OptiTrack measurement, IMU integration, and EKF-obtained values, for the body velocities (u, v, w) and attitude angles (Φ, Θ, Ψ)

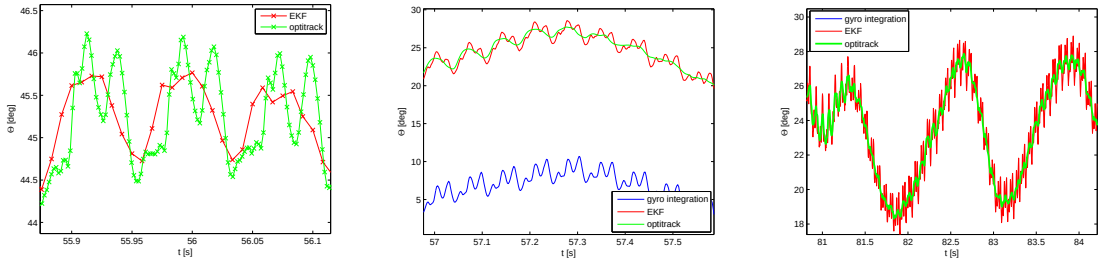

(a) (b) (c)

Figure 6: Detail of EKF results compared to OptiTrack measurements: high-frequency content in pitch attitude.

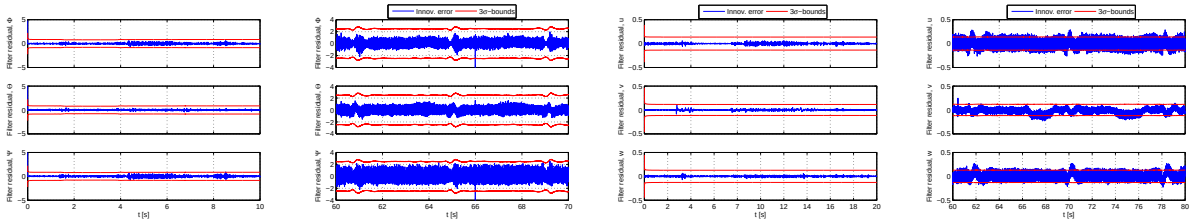

(a) Attitude, static condition (b) Attitude, free flight (c) Velocity, static condition (d) Velocity, free flight

Figure 7: EKF innovation errors and predicted error variance bounds ($\pm 3\sigma$) for the attitude and velocity components. Results are shown for both static and free-flight segments.

each other. In line with aerospace convention, the flight envelope was initially defined in terms of possible combinations of angle of attack and velocity, as well as the elevator deflection required to achieve these. For flapping-wing vehicles specifically, an additional important parameter to consider is the flapping frequency. This could be seen as an additional state, which defines the flight envelope together with the angle of attack and velocity, but could equally be seen as an input, as it is almost entirely a forced motion, in this case controlled directly via the motor RPM. In either case, there is a clear correlation between angle of attack, velocity, elevator deflection and flapping frequency, with increasing angles of attack implying decreasing velocities and increasing flapping frequencies, as can be seen in the figure.

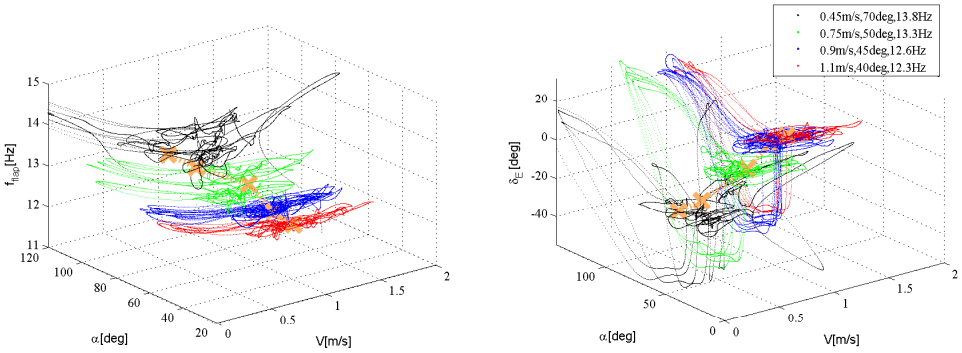

(a) Velocity, angle of attack and flapping frequency (b) Velocity, angle of attack and elevator deflection

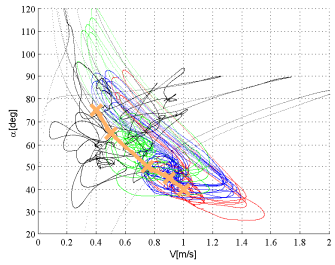

(c) Velocity and angle of attack

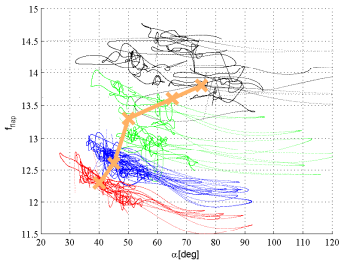

(d) Angle of attack and flapping frequency

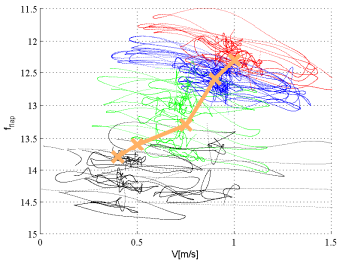

(e) Velocity and flapping frequency

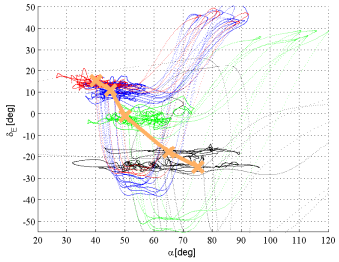

(f) Angle of attack and elevator deflection

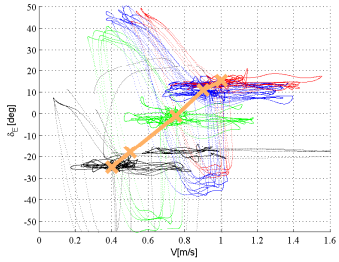

(g) Velocity and elevator deflection

Figure 8: Flight envelope representations – coverage obtained in the test flights, in terms of angle of attack, velocity ($||V||$), elevator deflection and flapping frequency. The 2D plots are projections of the 3D plots at the top. The nominal trim conditions defined in table 4 are shown in orange.

Another relevant consideration is that the ornithopter - like most flying vehicles - has an optimal operating range, where its performance is at its highest level. Moving away from this domain, flight is still possible but becomes increasingly difficult. This also helps to explain why results are significantly more consistent for conditions close to the ideal operating condition, while they vary more as we move away from this condition.

A first evaluation using the obtained flight data was made in order to establish the behaviour of the ornithopter in the different conditions covered, representing a significant part of the flight envelope of the

considered configuration (CG location). For this, the cycle-averaged behaviour of the system was considered, with the flapping component neglected under the assumption of time-scale separation, found to be sufficiently valid for high-level dynamic analysis for this ornithopter.[24] Subsequently, the time-varying, flapping-related component was briefly considered. Accurate measurement of the latter component represents one of the key contributions of the current experimental setup. The obtained insight and results are discussed in the following sections.

A. Dynamic analysis across the flight envelope

Evaluation of the time-averaged dynamics was conducted first visually, and, then using a data-driven modelling approach. Since results obtained at $0.4m/s$ and $0.5m/s$ were found to be very close and fewer manoeuvres were available for each of these test conditions, the two conditions were combined in the final evaluation.

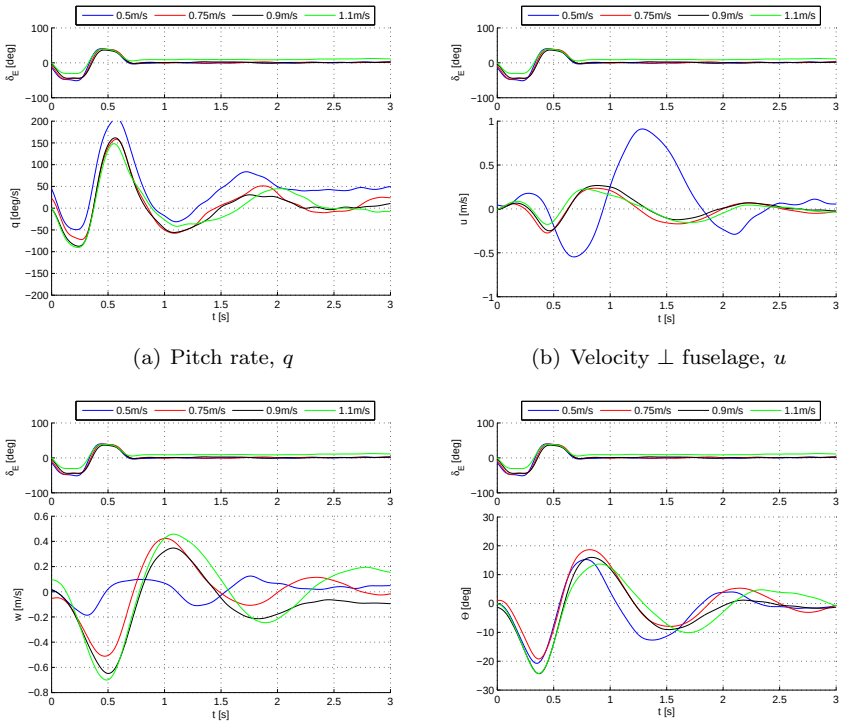

(a) Pitch rate, q

(b) Velocity $\perp$ fuselage, u

(c) Velocity $\parallel$ fuselage, w

(d) Pitch attitude, Θ

Figure 9: Typical responses of the ornithopter in the different flight regimes considered.

To start with, and to obtain a qualitative idea of the dynamics, the output itself was considered, in order to (i) evaluate visually how much the dynamics change between different conditions, and (ii) evaluate how similar the response to separate but similar manoeuvres conducted in the approximate same conditions is. Fig. 10 shows the response of the ornithopter in one particular flight condition, to eight separate manoeuvres. It can be seen that while not identical, the responses are very similar in separate manoeuvres. Fig. 9 presents an example of responses of the ornithopter to similar manoeuvres, in different flight regimes. It can be observed that changes are not linear - in fact the two central conditions are generally very close, with the highest and especially the lowest velocities leading to more widely differing responses. Nonetheless it should also be considered that the scales considered are small, and even a seemingly small difference can have a significant impact.

The dynamics were then analysed further with the help of modelling tools to obtain a more in-depth qualitative and quantitative overview. While flapping-wing dynamics are complex, warranting the investigation into multi-body models,[47,26,48,49] several studies have demonstrated that for basic flight dynamic considerations, e.g. in the context of design and control studies, the standard aircraft equations of motion yield a suitable description for many insects/ FWMAVs.[50,51,52,24] Thus, we used simple linear equations

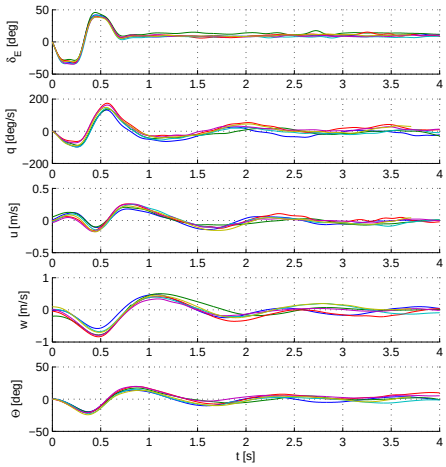

Figure 10: Comparison of different responses (perturbations) to the same manoeuvre, for one flight condition (1.1m/s)

as a tool to analyse the dynamics of the ornithopter. Assuming a simple, linear time-invariant (LTI) model structure, models for the longitudinal dynamics were identified for each manoeuvre conducted at each of the flight conditions considered. As in previous research on a similar FWMAV,[24] these local linear models were assumed to have the following structure,

$$\begin{bmatrix} \Delta\dot{q} \\ \Delta\dot{u} \\ \Delta\dot{w} \\ \Delta\dot{\Theta} \end{bmatrix} = \begin{bmatrix} \frac{M_q}{I_{yy}} & \frac{M_u}{I_{yy}} & \frac{M_w}{I_{yy}} & 0 \\ \frac{X_q}{m} - w_0 & \frac{X_u}{m} & \frac{X_w}{m} & g\cos(\Theta_0) \\ \frac{Z_q}{m} + u_0 & \frac{Z_u}{m} & \frac{Z_w}{m} & g\sin(\Theta_0) \\ 1 & 0 & 0 & 0 \end{bmatrix} \begin{bmatrix} \Delta q \\ \Delta u \\ \Delta w \\ \Delta\Theta \end{bmatrix} + \begin{bmatrix} \frac{M_{\delta_e}}{I_{yy}} & \frac{M_{\delta_f}}{I_{yy}} \\ \frac{X_{\delta_e}}{m} & \frac{X_{\delta_f}}{m} \\ \frac{Z_{\delta_e}}{m} & \frac{Z_{\delta_f}}{m} \\ 0 & 0 \end{bmatrix} \begin{bmatrix} \Delta\delta_e \\ \Delta\delta_f \end{bmatrix} \tag{26}$$

Since at this stage tests were only conducted using elevator input (cf. III), the flapping frequency-related parameters in the B-matrix could not be fully determined. However, sufficient excitation was still obtained to compute the A matrix. Preliminary tests with throttle manoeuvres showed that some components of the dynamics may be better excited by throttle signals, particularly the Z-force component, hence this will be investigated in future work. However, the overall improvement was found to be limited.

The parameters in eq. 26 were obtained by means of a maximum likelihood estimation process, as outlined in ref.[24] As in the reference, the identification data was decomposed into time-averaged and time-varying components, to simplify the modelling task, and only the time-averaged component was used to evaluate the time-averaged dynamics. Future work will encompass merging the two components and introducing the flapping dynamics into the overall model. In this regard, it was found in these tests that data, which have been heavily filtered to remove most of the flapping-related contribution, are firstly, more likely to lead to an accurate result (in terms of predictive capability and statistical properties), and, secondly, appear less likely to lead to divergence of the estimator. Thus, it is advised to use filtered data for identification of cycle-averaged dynamics of systems, like ornithopters, that incorporate two sufficiently different time scales, where the fast time scale can be considered noise. However, an alternative approach is required if it is of interest to model the fast time scale and its interaction with the slow time scale.

Fig. 11 shows the identification results obtained from one example manoeuvre in each different flight condition, compared to the measured flight data. It can be seen that a high accuracy is achieved. This was found to be the case for all datasets (e.g. average output correlation coefficient 0.96 considering all states), suggesting that for reasonable inputs the longitudinal system dynamics can be well-approximated by LTI model structures, even in different flight conditions, within the range considered in the tests.

Fig. 12 shows the poles of each estimated model, with different colours indicating models obtained in approximately the same flight conditions and each point representing a different manoeuvre. This yields an initial idea of the dynamics of the vehicle. It can be observed that in most cases the ornithopter exhibits

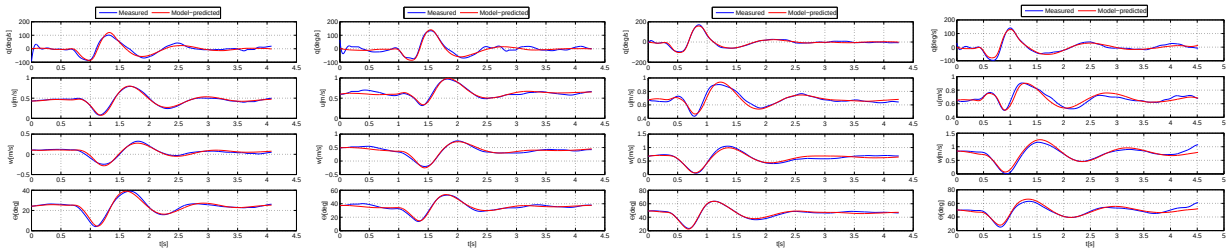

Figure 11: Example of measured and model-estimated states for one dataset in each condition considered.

one mostly stable oscillatory pole and two stable aperiodic poles, and, as expected, there is some variation between different flight conditions. Qualitatively, the dynamic behaviour is comparable to results in the literature for a different insects and FWMAVs in both experiment and simulation,[52,51,5] with the difference that the oscillatory mode is often found to be unstable in insects. The stability is a consequence of the tail on the studied ornithopter.

As can be seen in the figure, the oscillatory dynamics are captured accurately. Poles are clustered for similar conditions, with only slight overlap between results from different but neighbouring test conditions. Given the free-flight test conditions and manual trimming and piloting, it is unlikely for the exact same results to be obtained from any two distinct manoeuvres, however the generally good agreement between results obtained in the approximate same condition represents a form of validation and points to an adequate reliability of the results. It can also be observed that there is a clear trend in the oscillatory component. With increasing velocity, the oscillatory pole moves towards lower frequencies. It also appears to shift towards the right half plane, suggesting that at even higher velocities the oscillation may become unstable, while it becomes more stable at lower velocities. The damping seems fairly constant, except at the lowest velocity, where it appears to decrease. However, at very low velocities, the dynamics change significantly, and a significant second oscillation forms, so that evaluating the results becomes less straightforward. In general, the slow flight case leads to more widely varying results. This may have a number of causes. At low velocities the effect of disturbances, such as slight air draughts, becomes more significant. This also implies that velocity measurements, and hence computed angle of attack values, are less accurate, which may also affect the results. A visual evaluation during flight also suggests that the coupling between lateral and longitudinal dynamics is increased, and coupled oscillations tend to form, which the current model structure does not account for. Finally, it was remarked that at low velocities there was more noise in the data - this may have been partially related to the specific time the flights were conducted at (e.g. more light disturbing the tracking, more air fluctuations), but may also be connected to slow flight regimes, which can be more challenging to maintain smoothly. Hence more accurate testing and more complex model structures may be necessary to obtain a more elaborate idea of the dynamics at very low velocities.

The aperiodic dynamics are captured less accurately overall. It can be seen that there is a significant degree of variation, again, especially at very low velocities, where the aperiodic poles cover a wide range. There still appears to be a trend with the flight conditions, but it is more difficult to recognise clearly, and more data is required for a conclusive evaluation. In addition to the points discussed previously with regard to slow velocities, the larger variation in the aperiodic dynamics may also be due to insufficient excitation of parts of the dynamics - e.g. previous tests showed that throttle manoeuvres are required to excite some parts of the dynamics (mainly the velocity w, aligned with the fuselage) more effectively. Despite the significant uncertainty in the results, particularly for some of the tests, the aperiodic poles cover a fairly limited range, several results are repeatable and there do appear to be trends. Specifically, it seems that at very high velocities the aperiodic poles are closer together and stable, and in some cases they pair up to form a second, lower frequency and more damped oscillation. As the forward velocity increases, the poles move away from each other on the real axis. This trend is difficult to confirm with the current data, as there is some overlap, but certainly the poles vary more widely as the velocity increases. This may partly be due to inaccurate estimation and/or data, but also suggests that poles indeed become more spaced out. Moreover it can be seen that at very low velocities the vehicle appears to have a tendency to instability, and again, a second oscillatory pair seems to form, that has a similar damping to the first oscillation, but a lower frequency. This is in agreement with flight experience, where the vehicle has indeed been found to perform unusual, slow, badly damped oscillations at low velocities. These were mainly observed in the lateral dynamics, but

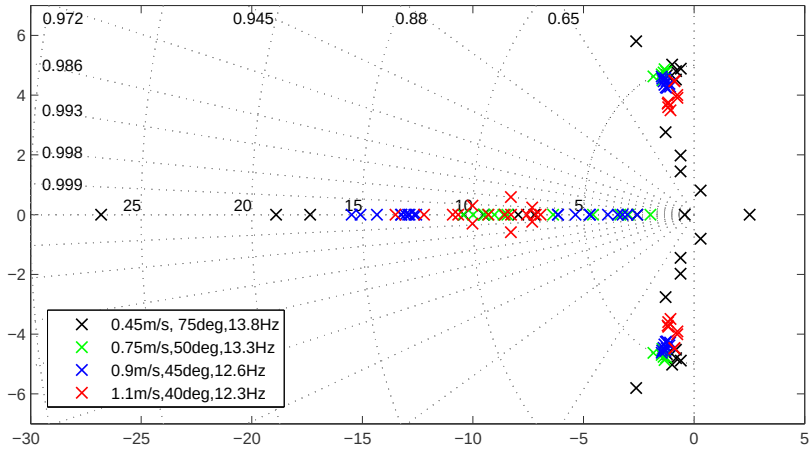

(a) Full overview of identified poles.

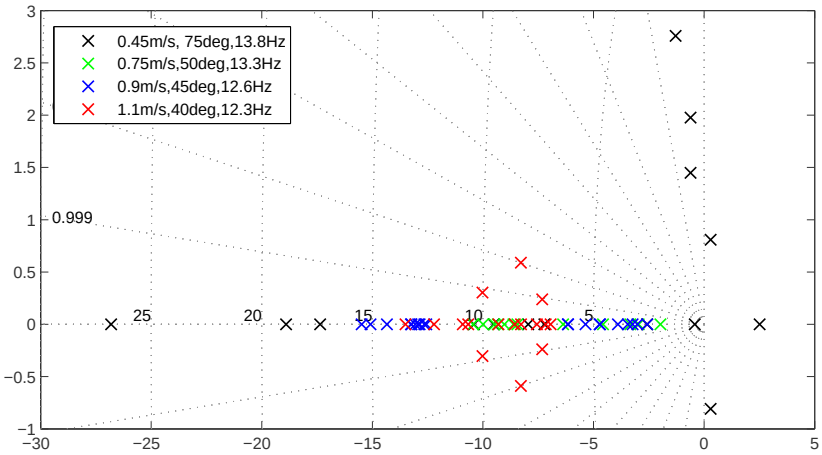

(b) Detail: real poles.

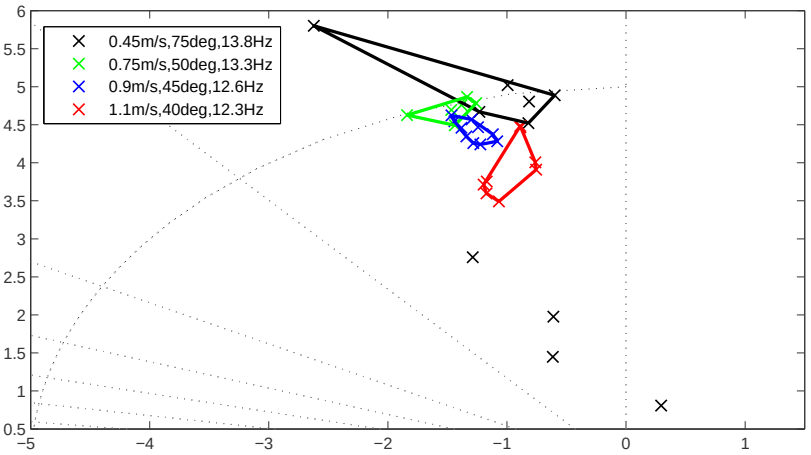

(c) Detail: imaginary poles; clusters of poles obtained in the same condition are highlighter for easier interpretation.

Figure 12: Poles of the models obtained in different conditions, from a number of different manoeuvres. Colours indicate results obtained in the same flight condition.

it is not unreasonable to suppose that something analogous is occurring to a lesser extent in the longitudinal dynamics, or indeed, that the two components become more coupled at low velocities.

Further testing is required to obtain a more conclusive, reliable and complete overview, however the current results already yield initial insight and represent a useful basis for further dynamic analysis and modelling.

B. Outlook: flapping behaviour analysis

In addition to supplying useful information on the cycle-averaged dynamics, the collected free-flight data can be used to effectively analyse sub-flap cycle processes. The suggested experimental setup allows for consideration of higher frequency content than can be achieved with optical tracking alone (cf. fig. 6), and allows for consideration of manoeuvres, which is not possible in open-loop wind tunnel experiments. Accurate and realistic high-frequency content can be useful for dynamic analysis, e.g. considering the effect of the flapping-related oscillations in the states, however it is particularly essential in aerodynamic studies. It has for instance been shown that some unsteady effects, such as clap-and-fling, are visible clearly only at very high frequencies,[14] which are typically only accurately observable in wind tunnel tests. At the same time, as mentioned in sec. I, wind tunnel and free-flight data are not always identical, hence it is valuable to be able to obtain qualitatively comparable data in free-flight conditions. The suggested EKF yields results that are closer to wind tunnel results in terms of detail and information content, while also more realistic, as they represent free flight. The possibility of considering manoeuvres is also of interest, as this is an essential component for a real flying vehicle. Furthermore, previous work has hypothesised that additional interactions may occur at the sub-flap level during manoeuvres, that are not observable in steady flight. Again, this cannot be studied in the wind tunnel. Thus, the suggested combination of different data sources yields a more comprehensive and in-depth overview of time-resolved flapping behaviour, that constitutes a useful stepping stone for further work in this field.

V. Conclusion

We discussed a set of flight tests conducted for dynamic analysis and model identification of a flapping-wing micro aerial vehicle (FWMAV) in different flight regimes, ranging from 0.4 to 1.1 m/s. The flight test planning and execution was discussed, including experiment design and data fusion procedures specific to flapping-wing vehicles, and, in some cases, applying equally to MAVs in general. A number of issues were identified, and solutions suggested where available.

An extended Kalman filter was suggested to fuse data from on-board inertial sensors and off-board optical tracking measurements. This was found to provide more reliable data and, in particular, to yield more extensive and accurate insight into the sub-flap cycle behaviour of the vehicle. This approach is considered generally useful for studying flapping-wing vehicles in free-flight, as it avoids the tethering inherent in wind tunnel testing and also allows for manoeuvring to be considered.

System identification was applied to obtain simple linear models for the flight dynamics of the vehicle in each of the different flight regimes considered. All obtained models were found to be accurate, and, additionally, models obtained from separate manoeuvres conducted in the same flight condition, generally led to comparable results. An initial global evaluation was made by comparing the eigenmodes of the obtained models, hence gaining some insight into the dynamics of the platform. The ornithopter was found to have a periodic mode and two aperiodic modes. The periodic mode assumes decreasing frequencies at increasing trimmed forward velocities, and tends to become less damped and less stable at very low velocities. Similar results are obtained for the same flight conditions. The aperiodic modes vary model widely, both within the same flight conditions and between different flight conditions, and improved results may be obtained through the use of additional excitation through flapping frequency variation input signals, as well as more accurate testing. Current results suggest that the two aperiodic modes are close together on the real axis at high velocities, and move further apart as velocity decreases, forming a second oscillatory mode at very low velocities, and tending towards instability. However, further testing is required to confirm these observations.

The obtained results pave the way for global modelling, providing an initial dataset that covers a range of different conditions, and also includes accurate flapping effects. Future work will encompass extending the reach of the dataset, by considering different centre of gravity locations, as well as lateral dynamics, and integrating flapping effects in the model. Flapping frequency input will also be used to provide more effective

excitation of certain components in the dynamics, as well as to obtain an idea of the control effectiveness of the flapping wings, whose frequency can be varied while flying. The final goal is to develop a comprehensive global model by combining the local models, thus expanding the potential of the vehicle studied, but also yielding insight into flapping-wing mechanisms and design generally. A global model will also be a significant asset for control design work, allowing for more effective controllers, and ultimately, improved autonomy and performance of flapping-wing flyers.

References

[1]Ellington, C. P., "The Aerodynamics of Hovering Insect Flight. I. The Quasi-Steady Analysis," *Philosophical Transactions of the Royal Society B: Biological Sciences*, Vol. 305, No. 1122, Feb. 1984, pp. 1–15.

[2]Ellington, C., van den Berg, C., Willmott, A., and Thomas, A., "Leading-edge vortices in insect flight," *Nature*, Vol. 384, No. 19/26, 1996, pp. 626–630.

[3]Sane, S. P., "The aerodynamics of insect flight," *Journal of Experimental Biology*, Vol. 206, No. 23, Dec. 2003, pp. 4191–4208.

[4]Dickinson, M. H., Lehmann, F., and Sane, S. P., "Wing Rotation and the Aerodynamic Basis of Insect Flight," *Science*, Vol. 284, No. 5422, June 1999, pp. 1954–1960.

[5]Taylor, G. K., "Dynamic flight stability in the desert locust Schistocerca gregaria," *Journal of Experimental Biology*, Vol. 206, No. 16, Aug. 2003, pp. 2803–2829.

[6]Dietl, J., Herrmann, T., Reich, G., and Garcia, E., "Dynamic Modeling, Testing, and Stability Analysis of an Ornithoptic Blimp," *Journal of Bionic Engineering*, Vol. 8, No. 4, Dec. 2011, pp. 375–386.

[7]Doman, D. B., Oppenheimer, M. W., and Sigthorsson, D. O., "Dynamics and control of a minimally actuated biomimetic vehicle: part I - aerodynamics model," 2011.

[8]Grauer, J., Ulrich, E., Jr., J. H., Pines, D., , and Humbert, J. S., "Testing and System Identification of an Ornithopter in Longitudinal Flight," *Journal of Aircraft*, Vol. 48, No. 2, March-April 2011, pp. 660–667.

[9]Han, J.-s., Chang, J. W., Kim, J.-k., and Han, J.-H., "Experimental Study on the Unsteady Aerodynamics of a Robotic Hawkmoth Manduca sexta model," *AIAA SciTech 13-17 January 2014, National Harbor, Maryland, 52nd Aerospace Sciences Meeting*, No. January, 2014, pp. 1–9.

[10]Lee, J.-S. and Han, J.-H., "Experimental study on the flight dynamics of a bioinspired ornithopter: free flight testing and wind tunnel testing," *Smart Materials and Structures*, Vol. 21, No. 9, Sept. 2012, pp. 094023.

[11]Nakata, T., Liu, H., Tanaka, Y., Nishihashi, N., Wang, X., and Sato, A., "Aerodynamics of a bio-inspired flexible flapping-wing micro air vehicle," *Bioinspiration & Biomimetics*, Vol. 6, 2011.

[12]Percin, M., Eisma, H., van Oudheusden, B., Remes, B., Ruijsink, R., and de Wagter, C., "Flow Visualization in the Wake of the Flapping-Wing MAV 'DelFly II' in Forward Flight," *AIAA Applied Aerodynamics Conference*, AIAA, 2012.

[13]Caetano, J. V., Weehuizen, M. B., de Visser, C. C., de Croon, G. C. H. E., and Mulder, M., "Rigid-Body Kinematics Versus Flapping Kinematics of a Flapping Wing Micro Air Vehicle," *Journal of Guidance, Control and Dynamics*, Vol. 38, No. 12, Dec. 2015, pp. 2257–2269.

[14]Armanini, S. F., Caetano, J. V., de Croon G. C. H. E., de Visser, C. C., and Mulder, M., "Quasi-Steady Aerodynamic Model of Clap-and-Fling Flapping MAV and Validation using Free-Flight Data," *Bioinspiration & Biomimetics*, (in press).

[15]Caetano, J. V., Percin, M., van Oudheusden, B. W., Remes, B. D. W., de Wagter, C., de Croon, G. C. H. E., and de Visser, C. C., "Error Analysis and Assessment of Unsteady Forces Acting on a Flapping Wing Micro Air Vehicle: Free-Flight versus Wind Tunnel Experimental Methods," *Bioinspiration & Biomimetics*, Vol. 10, No. 5, 2015.

[16]Jennings, A., Mayhew, M., and Black, J., "Video measurements of instantaneous forcesof flapping wing vehicles," *Mechanical Systems and Signal Processing*, Vol. 64-65, No. 2015, Dec. 2015, pp. 325336.

[17]Rose, C. and Fearing, R. S., "Comparison of Ornithopter Wind Tunnel Force Measurements with Free Flight," *2014 IEEE International Conference on Robotics & Automation (ICRA)*, IEEE, May-June 2014, pp. 1816–1821.

[18]Grauer, J., Ulrich, E., Hubbard, J. E., Pines, D., and Humbert, J. S., "Testing and System Identification of an Ornithopter in Longitudinal Flight," *Journal of Aircraft*, Vol. 48, No. 2, March 2011, pp. 660–667.

[19]Finio, B. M., Perez-Arancibia, N. O., and Wood, R. J., "System identification and linear time-invariant modeling of an insect-sized flapping-wing micro air vehicle," *2011 IEEE/RSJ International Conference on Intelligent Robots and Systems*, Ieee, Sept. 2011, pp. 1107–1114.

[20]Duan, H. and Li, Q., "Dynamic model and attitude control of Flapping Wing Micro Aerial Vehicle," *2009 IEEE International Conference on Robotics and Biomimetics (ROBIO)*, Dec. 2009, pp. 451–456.

[21]Chand, A. N., Kawanishi, M., and Narikiyo, T., "Parameter Estimation for the Pitching Dynamics of a Flapping-Wing Flying Robot," *IEEE International Conference on Advanced Intelligent Mechatronics (AIM)*, Busan, Korea, 2015, pp. 1552–1558.

[22]Caetano, J. V., de Visser, C. C., de Croon, G. C. H. E., Remes, B. D. W., de Wagter, C., Verboom, J. L., and Mulder, M., "Linear Aerodynamic Model Identification of a FlappingWing MAV Based on Flight Test Data," *International Journal of Micro Air Vehicles*, Vol. 5, No. 4, December 2013, pp. 273–286.

[23]Armanini, S. F., de Visser, C. C., and de Croon, G. C. H. E., "Black-box LTI modelling of flapping-wing micro aerial vehicle dynamics," *AIAA Atmospheric Flight Mechanics Conference*, Kissimee, FL, USA, Jan. 2015, AIAA Paper 15-0234.

[24]Armanini, S. F., Visser, C. C. D., Croon, G. C. H. E. D., and Mulder, M., "Time-varying model identification of flapping-wing vehicle dynamics using flight data," *Journal of Guidance, Control, and Dynamics*, Vol. 39, No. 3, 2016, pp. 526–541.

[25]Berman, G. J. and Wang, Z. J., "Energy-minimizing kinematics in hovering insect flight," *Journal of Fluid Mechanics*, Vol. 582, June 2007, pp. 153–168.

[26]Orlowski, C. T., "Stability Derivatives for a Flapping Wing MAV in a Hover Condition Using Local Averaging," 2011, pp. 1604–1609.

[27]Xiong, Y. and Sun, M., "Stabilization control of a bumblebee in hovering and forward flight," *Acta Mechanica Sinica*, Vol. 25, No. 1, 2009, pp. 13–21.

[28]Wu, J. and Sun, M., "Control for going from hovering to small speed flight of a model insect," *Acta Mechanica Sinica*, Vol. 25, No. 3, 2009, pp. 295–302.

[29]de Croon, G. C. H. E. D., de Clercq, K. M. E. D., Ruijsink, R., Remes, B., de Wagter, C., and Croon, G. C. H. E. D., "Design, aerodynamics, and vision-based control of the DelFly," *International Journal of Micro Air Vehicles*, Vol. 1, No. 2, 2009, pp. 71–98.

[30]de Croon, G. C. H. E., Groen, M. a., De Wagter, C., Remes, B., Ruijsink, R., and van Oudheusden, B. W., "Design, aerodynamics and autonomy of the DelFly." *Bioinspiration & biomimetics*, Vol. 7, No. 2, June 2012, pp. 025003.

[31]Caetano, J. V., "Near-Hover Flapping Wing MAV Aerodynamic Modelling - a linear model approach," , No. September, 2013, pp. 17–20.

[32]Remes, B. D. W., Esden-Tempskiy, P., van Tienen, F., Smeur, E., De Wagter, C., and de Croon, G. C. H. E., "Lisa-S 2.8g autopilot for GPS-based flight of MAVs," *International Micro Air Vehicle Conference and Competition (IMAV)*, Delft, The Netherlands, 2014, pp. 280–285.

[33]"http://wiki.paparazziuav.org," website.

[34]Caetano, J. V., Weehuizen, M. B., Visser, C. C. D., Croon, G. C. H. E. D., and Wagter, C. D., "Rigid vs . Flapping : The Effects of Kinematic Formulations in Force Determination of a Free Flying Flapping Wing Micro Air Vehicle," .

[35]Karásek, M., Koopmans, A. J., Armanini, S. F., Remes, B. D. W., and de Croon G. C. H. E., "Free Flight Force Estimation of a 23.5 g Flapping Wing MAV using an on-board IMU," *International conference on intelligent robots and systems (IROS)*, Daejeon, Korea, 2016, (submitted).

[36]Armanini, S. F., Verboom, J. L., de Croon, G., and de Visser, C., "Determination of trim curves for a flapping-wing MAV," *International Micro Air Vehicles Conference and Competition IMAV*, Delft, 2014, pp. 212–217.

[37]Mulder, J., *Design and evaluation of dynamic flight test manoeuvres*, Phd, 1986.

[38]Plaetschke, E. and Schulz, G., "Practical input signal design," *Parameter Identification AGARD-LS-104*, NATO, 1979.

[39]Maine, R. and Iliff, K., "Application Of Parameter Estimation To Aircraft Stability And Control: The Output-Error Approach," Nasa reference publication 1168, NASA, 1986.

[40]Klein, V. and Morelli, E., *Aircraft System Identification*, AIAA Education Series, 2006.

[41]Iliff, K. W., "Identification of Aircraft Stability and Control Derivatives in the Presence of Turbulence," Tech. rep., NASA TN D-7647, 1974.

[42]Milne, G., Mulder, J., Soijer, M., Juliana, S., and Hermansyah, "Maximum Likelihood Stability and Control Derivative Identification of a Cessna Citation II," *AIAA Atmospheric Flight Mechanics Conference and Exhibit, Montreal, Canada*, 2001.

[43]Napolitano, M., Paris, A., Seanor, B., and Bowers, A., "Parameter Estimation for a Cessna U-206 Aircraft Using the Maximum Likelihood Method," *AIAA*, , No. 94-3481, 1994.

[44]Koopmans, A., *Delfly Freeflight: Autonomous flight of the DelFly in the wind tunnel using low-cost sensors*, Master's thesis, Delft University of Technology, http://www.delfly.nl/?site=Publications&menu=&lang=en, 2012.

[45]Jategaonkar, R., *Flight Vehicle System Identification A Time Domain Methodology*, AIAA Progress in Astronautics and Aeronautics, Reston, VA, USA, 2006.

[46]Plaetschke, E. and Schulz, G., "Practical input signal design. Parameter Identification. AGARD-LS-104, November 1979, Paper No. 3," Tech. rep., NATO.

[47]Orlowski, C., Girard, A., Shyy, W., and Arbor, A., "Derivation and simulation of the nonlinear dynamics of a flapping wing micro-air vehicle," .

[48]Bolender, M. A., "Rigid Multi-Body Equations-of-Motion for Flapping Wing MAVs using Kane Equations," *AIAA Guidance, Navigation, and Control Conference*, No. 2009-6158, August 2009.

[49]Grauer, J. A., Hubbard, J. E., and Jr, J. E. H., "Multibody Model of an Ornithopter," *Journal of Guidance, Control, and Dynamics*, Vol. 32, No. 5, Sept. 2009, pp. 1675–1679.

[50]Taylor, G. K. and Thomas, A. L. R., "Dynamic flight stability in the desert locust Schistocerca gregaria," *Journal of Experimental Biology*, Vol. 206, No. 16, Aug. 2003, pp. 2803–2829.

[51]Sun, M. and Xiong, Y., "Dynamic flight stability of a hovering bumblebee." *The Journal of experimental biology*, Vol. 208, No. Pt 3, Feb. 2005, pp. 447–59.

[52]Faruque, I. and Sean Humbert, J., "Dipteran insect flight dynamics. Part 1 Longitudinal motion about hover." *Journal of theoretical biology*, Vol. 264, No. 2, May 2010, pp. 538–52.